Appl. Phys. B
DOI 10.1007/s00340-014-5809-y

Applied Physics B
Lasers and Optics

Quartz-enhanced photoacoustic spectroscopy-based sensor system for sulfur dioxide detection using a CW DFB-QCL

J. P. Waclawek · R. Lewicki · H. Moser · M. Brandstetter · F. K. Tittel · B. Lendl

Received: 17 December 2013 / Accepted: 24 February 2014

Abstract Sulfur dioxide (SO_2) trace gas detection based on quartz-enhanced photoacoustic spectroscopy (QEPAS) using a continuous wave, distributed feedback quantum cascade laser operating at 7.24 μm was performed. Influence of water vapor addition on monitored QEPAS SO_2 signal was also investigated. A normalized noise equivalent absorption coefficient of NNEA (1σ) = 1.21×10^{-8} cm^{-1} W Hz$^{-1/2}$ was obtained for the ν_3 SO_2 line centered at 1,380.93 cm^{-1} when the gas sample was moisturized with 2.3 % H_2O. This corresponds to a minimum detection limit (1σ) of 63 parts per billion by volume for a 1 s lock-in time constant.

1 Introduction

1.1 Quartz-enhanced photoacoustic spectroscopy

Laser-based photoacoustic spectroscopy (PAS) is a well-known technique for detection of trace chemical species in the gas phase providing high sensitivity and selectivity [1, 2]. PAS trace gas analysis finds applications in diverse fields such as environmental monitoring, industrial process control or medical diagnostics [3–5]. The absorption of modulated laser radiation by gas molecules causes heating of the chemical species which results in thermal expansion and leads to a pressure change in the targeted media. For modulated laser light, this generated pressure waves can be detected by an acoustic transducer. Conventional PAS employs sensitive microphones placed into resonant cells that have typically volumes greater than 10 cm^3 [6]. A variation of the traditional PAS approach uses a quartz tuning fork (QTF) as a sharply resonant piezoelectric acoustic transducer with an extremely high quality factor (Q-factor) of >10,000, instead of a broadband electric microphone and a relatively low Q-factor ($\sim$200) resonant photoacoustic cell. This technique is known as quartz-enhanced photoacoustic spectroscopy (QEPAS) and was first reported in 2002 [7]. The QTF is a low-loss piezoelectric element resonating at 32,768 (=2^{15}) Hz in vacuum and converts its deformation, caused by generated pressure waves, into separation of electrical charges that can be measured either as voltage or current. Due to the small size of the QTF, the QEPAS technique facilitates the measurement of trace gases in an ultra-small acoustic detection module (ADM) with a total effective sample volume of only a few mm^3. Only the fundamental symmetric vibration of the QTF is piezoelectric active, i.e., when the two prongs bend in opposite directions in the plane of the QTF. Thus, in a typical arrangement the laser beam is focused between the prongs of the QTF in order to probe the acoustic waves and achieve the highest electric signal [1, 2, 8–10]. Acoustically the QTF is a quadruple, which results in excellent environmental noise immunity, because sound waves from distant acoustic sources tend to move the QTF prongs in the same direction, thus resulting in no electrical response. The detected QEPAS signal is directly proportional to the absorption coefficient per unit concentration of the target species, the concentration of the target species, the laser power, the Q-factor of the acoustic resonator and inversely proportional to the QTF frequency f_0 [11]. The pressure of the sample gas influences the Q-factor of the QTF, vibrational–translational (V–T) relaxation of the targeted

J. P. Waclawek · H. Moser · M. Brandstetter · B. Lendl (✉)
Institute of Chemical Technologies and Analytics, Vienna University of Technology, Getreidemarkt 9/164-UPA, 1060 Vienna, Austria
e-mail: bernhard.lendl@tuwien.ac.at

R. Lewicki · F. K. Tittel
Electrical and Computer Engineering Department, Rice University, MS-366; 6100 Main St., Houston, TX 77005, USA
e-mail: fkt@rice.edu

Published online: 06 April 2014

trace gas analyte, as well as the width of the absorption line and potential cross-interference with other species. In order to achieve the best QEPAS detection sensitivity and selectivity, it is necessary to select the optimum operating pressure for a QEPAS-based trace gas sensor system.

The generation of a photoacoustic wave is related to the vibrational–translational (V–T) relaxation in gases, i.e., the energy transfer from vibrationally excited molecular states to translational degrees of freedom. In case of a slow V–T relaxation with respect to the modulation frequency f_{mod} ($\omega\tau_{\mathrm{VT}} \gg 1$, where $\omega = 2\pi f_{\mathrm{mod}}$), the photoacoustic sound generation is suppressed because the excitation of the gas molecules is faster than the complete relaxation. Therefore, the generated photoacoustic wave is weaker than it would be in case of instantaneous V–T energy equilibrium. SO_2 is a comparatively slow relaxing molecule, and due to the fact that QEPAS uses a rather high modulation frequency of $\sim$16.384 kHz determined by the QTF, the detected signal amplitude is affected by the V–T relaxation rate of the target molecule. In a pure mixture of the trace chemical species in N_2, the vibrational energy can be transferred during collisions between SO_2 and N_2 molecules and also between SO_2 molecules themselves. Due to the strong dipole moment of the H_2O molecule, its addition to a sample gas mixture results in a V–T relaxation of excited molecules that is considerably faster and is therefore an efficient catalyst for the vibrational energy transfer reactions in the gas phase [12, 13]. Thus, the presence of H_2O vapor enhances the QEPAS response to SO_2 which results in higher amplitude of the detected signal.

In this work, the metrological qualities of the QEPAS detection are investigated with sulfur dioxide as the target analyte. SO_2 is a major air pollutant released into the atmosphere by both natural and anthropogenic sources, including industrial combustion processes, fuel-based transport activities as well as volcanic eruptions. SO_2 emissions are a precursor to acid rain and atmospheric particulates which affects vegetation, stratospheric chemistry and climate. Exposure to SO_2 in ambient air has been associated with various health symptoms, including reduced lung functions, increased incidence of respiratory diseases and premature mortality. The threshold of SO_2 impact on human health at brief exposures occurs when the SO_2 concentration exceeds 380 parts per billion by volume (ppbv) in ambient air [14].

2 Experimental

2.1 CW DFB-QCL performance and SO_2 wavelength selection

In this work, a high heat load (HHL) packaged continuous wave (CW), distributed feedback quantum cascade laser (DFB-QCL) (*L10195-7253H, Hamamatsu*) emitting at $\sim$7.24 μm was employed as a compact, efficient and powerful spectroscopic source generating up to 155 mW of optical radiation in the molecular fingerprint region. The DFB-QCL operated at a single-mode frequency and could be tuned over a few wave numbers by varying the QCL either by temperature or injection current. Coarse frequency tuning from 1,380.73 to 1,378.94 cm^{-1} at a fixed laser current of 800 mA could be achieved by increasing the laser temperature from 18 °C (291.2 K) to 30 °C (303.2 K). This results in the laser temperature tuning coefficient of approximately -0.149 cm^{-1} K^{-1}. Fine frequency tuning in the range of $\sim$1.77 cm^{-1} was accomplished by changing the laser current from 600 to 800 mA, which correlated to a current tuning coefficient of approximately -0.009 cm^{-1} mA^{-1}. The optical power of the collimated laser beam was measured by a commercial power meter (*Solo 2, Gentec-Eo*). Figure 1a depicts the injection current versus optical power characteristics of the CW DFB-QCL at four different temperatures. The QCL is capable of emitting an optical power as high as 155 mW when operated at a temperature of 18 °C and at an injection current of 800 mA. Figure 1b shows the emitted single-mode laser radiation spectra at different QCL currents but constant temperature of 18 °C and the inset shows a step scan recording of the modulated QCL beam. Both spectra were obtained by a FT-IR spectrometer (*Vertex 80v, Bruker Optics*) with an instrumental spectral resolution of 0.0749 cm^{-1}.

The most intense absorption band of SO_2 is located in the spectral region between 1,330 and 1,400 cm^{-1}, with the strongest line centered at 1,348.38 cm^{-1}. Figure 2a shows HITRAN2008 simulated absorption spectrum for the ν_3 fundamental band of SO_2 within the 7.3 μm spectral region [15]. Figure 2b depicts HITRAN2008 simulated absorption spectra of 10 ppm SO_2:N_2 and 2.5 % H_2O:N_2 within the spectral range covered by the CW DFB-QCL. In order to perform sensitive SO_2 QEPAS measurements, an absorption line centered at 1,380.93 cm^{-1} and a QCL operating temperature of 18 °C were selected, because of its high line intensity, good separation from other SO_2 lines, and no H_2O interference.

2.2 Sensor system architecture and operation principle

The QEPAS-based gas sensor system architecture employing a high heat load (HHL) packaged CW DFB-QCL as a spectroscopic source is depicted in Fig. 3. An anti-reflection (AR) coated aspheric collimating lens (*Black Diamond™*, effective focal length = 4 mm) was used to collimate the laser beam. The HHL QCL package consists of an anti-reflection (AR) coated ZnSe window placed coplanar to the QC chip. In order to improve the laser beam quality, a spatial filter consisting of a plano-convex CaF_2 lens ($f = 25$ mm)

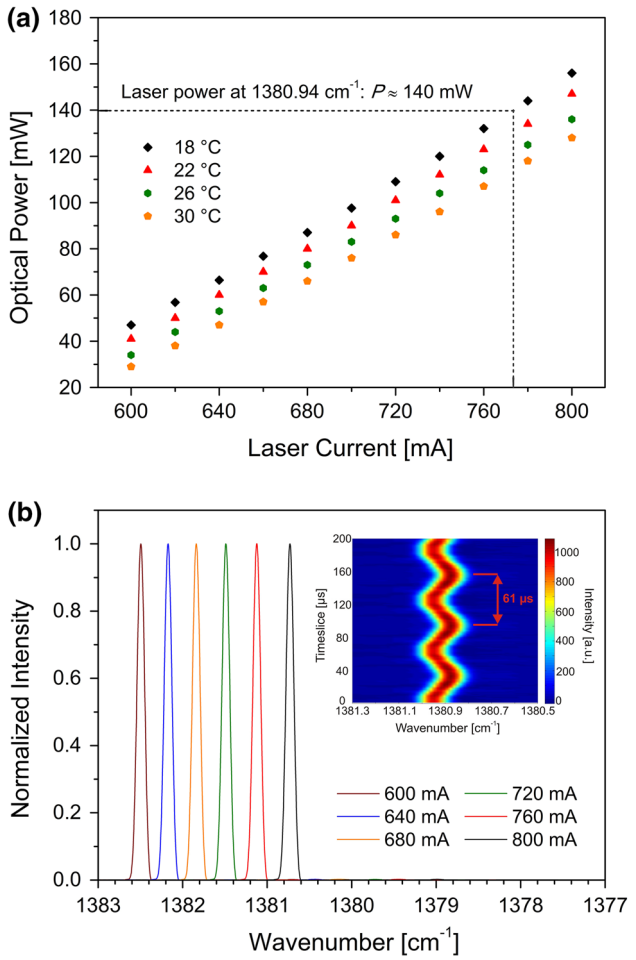

Fig. 1 **a** CW DFB-QCL output power and injection current tuning characteristics at four temperatures, **b** single-mode QCL output radiation for six injection currents at a fixed temperature of 18 °C; *Inset*: Step scan recording of the single-mode QCL radiation modulated with a frequency of 16.4 kHz and a modulation depth of $m = 0.072$ cm^{-1}

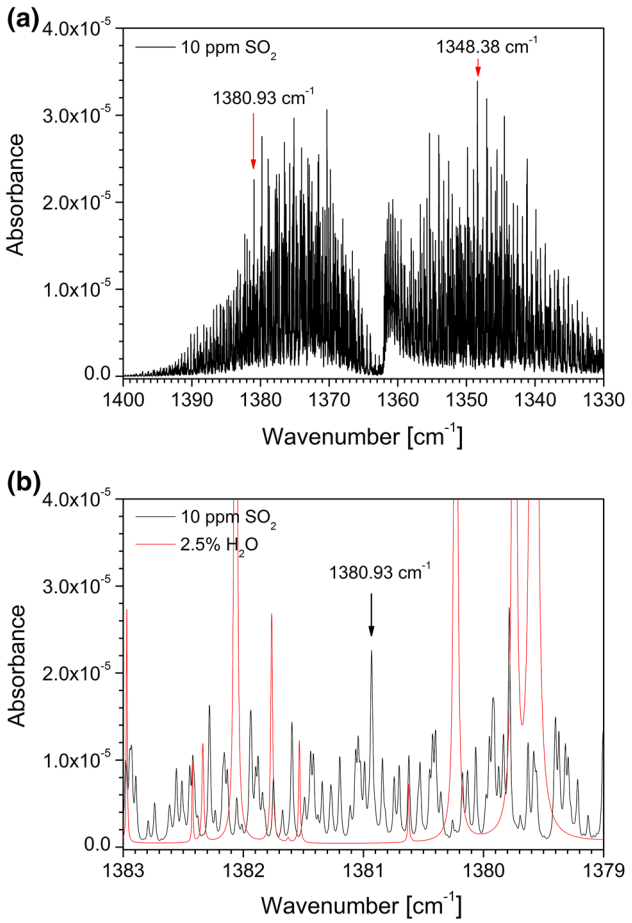

Fig. 2 **a** HITRAN2008 simulated spectra of 10 ppm SO_2 in N_2 and **b** HITRAN2008 simulated spectra of 10 ppm SO_2 and 2.5 % H_2O in N_2 within the wavelength tuning range of the 7.24 µm CW DFB-QCL ($p = 100$ mbar, $l = 1$ cm, $T = 296$ K)

and a 300-µm pinhole was implemented. The beam was focused with a second CaF_2 lens ($f = 25$ mm) into a compact QEPAS ADM gas cell, which consisted of a gas in- and outlet connectors, two ZnSe windows (AR coated) and the QTF used as an acoustic transducer. The Q-factor of the bare QTF used in this work was ~106,415 in vacuum and ~14,603 at atmospheric pressure, resulting in a change in the QTF resonant frequency from $f_0 = 32{,}763.8$ to $f_0 = 32{,}751.5$ Hz, respectively.

A further significant enhancement of the detected QEPAS signal can be achieved when two tubes acting as a micro-resonator (mR) are added to the QTF sensor architecture. For a near-IR fiber-coupled diode laser-based QEPAS system, an experimental optimization study of the geometrical mR parameters showed that the highest signal-to-noise ratio (SNR) is achieved for two 4.4 mm long and 0.5–0.6 mm inner diameter mR tubes [16]. However, when using mid-IR-free space optics, a lager inner diameter of the tubes is acceptable to simplify the alignment of the excitation beam through the mR tubes without significant reduction in the QEPAS signal. Therefore, two 4.4-mm-long stainless steel tubes with 0.84 mm inner diameter were used. Moreover, for better confinement of the propagating acoustic wave, a typical QEPAS configuration was used, where the QTF is positioned 30–50 µm from the end faces of the QTF mR tubes. The QCL beam was transmitted through the mR tubes and the gap between QTF prongs. Acoustic coupling between the mR and the piezoelectric QTF leads to an improved QEPAS-based trace gas sensor detection sensitivity of ~10 times.

A reference cell filled with 0.5 % SO_2:N_2 at a pressure of 133 mbar and a MCT detector (*PCI-2TE-12/MPAC-F-100*, *Vigo Systems S.A.*) located after the ADM were used as the reference channel in order to lock the laser frequency to the center of the selected SO_2 absorption line. The sensor platform was based on 2*f* wavelength modulation

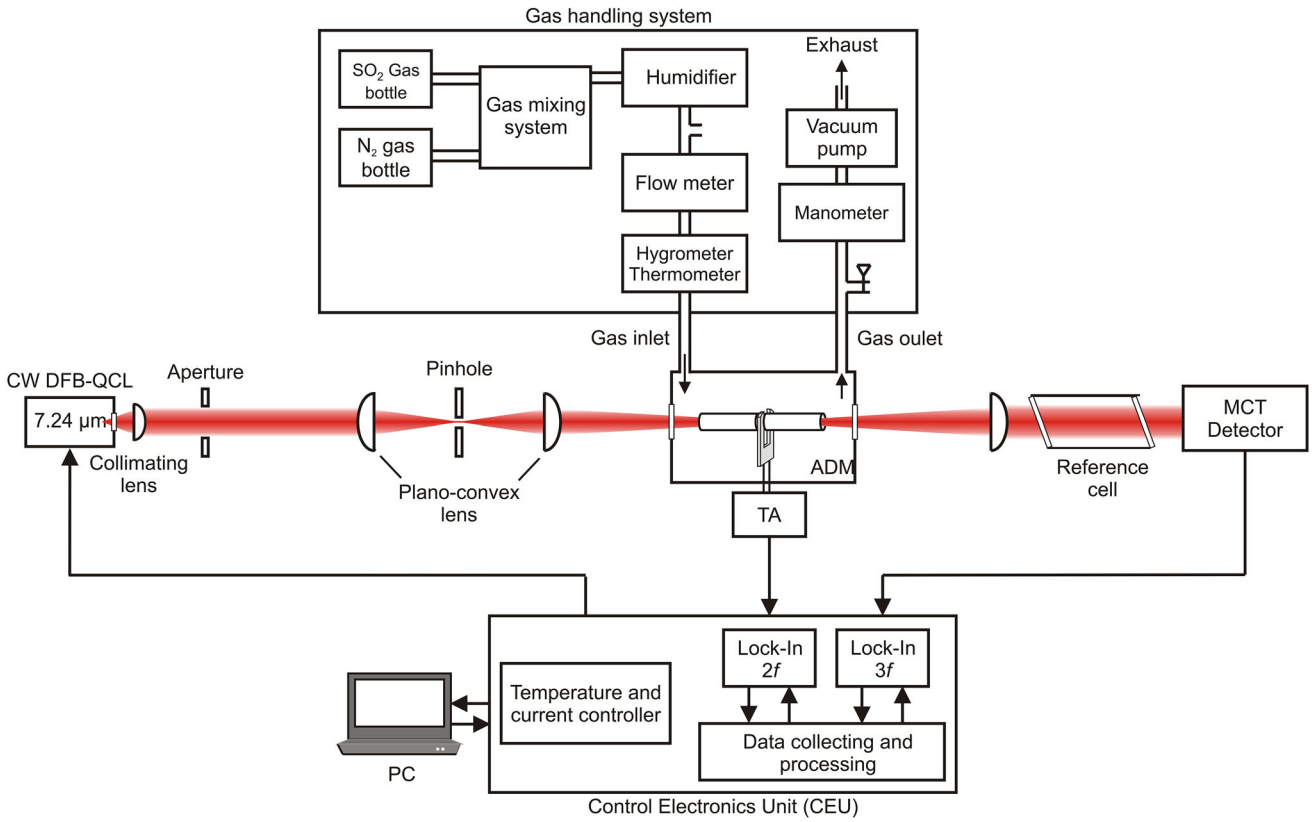

Fig. 3 Schematic diagram of the QEPAS-based SO_2 gas sensor employing a 7.24 µm CW DFB-QCL

spectroscopy (WMS) and QEPAS detection [8, 17]. The 2*f* WMS operation mode provides suppression of the acoustic background that is by nonselective absorbers. In this case, the noise level is primarily determined by the thermal noise of the QTF [18]. However, additional noise can be introduced by unintended illumination of the QTF by laser light, including any scattered light and incidental reflections from optical elements [11].

In order to implement the 2*f* WMS technique, the emission wavelength of the CW DFB-QCL was modulated at half of the QTF resonance frequency $f_{\mathrm{mod}} = f_0/2$ by embedding a sinusoidal modulation atop of the DC laser current. The detection of the QTF signal was performed at f_0, using an internal lock-in amplifier (LIA) with a time constant set to 1 s. The QEPAS detection was carried out in two modes: scan mode and locked mode. In the scan mode, the DC component of the QCL current is slowly tuned, so the laser frequency sweeps over the desired spectral range in order to acquire spectral information of the gas sample. In the locked mode, the QCL frequency is locked to the center of the SO_2 absorption line at 1,380.93 cm^{-1}, and a MCT detector signal is demodulated by a LIA at 3*f*. A proportional correction signal is applied to the DC component of the QCL to maintain the laser frequency at zero-crossing of the demodulated at 3rd harmonic MCT detector signal for the targeted SO_2 line. In this case, a continuous monitoring of the reference channel 3*f* signal helps to avoid any laser drift.

The acoustic waves interact with the QTF causing vibration of its prongs and therefore generate a piezoelectric current in the element. The piezoelectric current was converted to a voltage by a custom-made ultra-low noise transimpedance amplifier with a 10 MΩ feedback resistor and was subsequently transferred to a custom-made control electronics unit (*QEPAS Control Electronics Unit, CDP Systems Corp.*), which provides measurement of the QTF parameters, modulation of the laser current and measurement of the 2*f* component of the QTF and the 3*f* component of the photodetector signal. Further data processing was carried out with a LabVIEW-based program by transferring the digitized data to a computer.

2.3 Sample preparation system

Different SO_2 concentration levels within the range of 0–10 ppm were achieved by diluting a 50 ppm SO_2:N_2 calibration mixture with ultra-high purity N_2 using a custom-made gas mixing system. The N_2 used for dilution can be moisturized with water vapor in a range between 0 and ~88 % of a relative humidity when passing N_2 through the

gas phase of temperature controlled H_2O bath. The moisture was measured by a capacitive humidity sensor (*KFS150, Hygrosens*) and could be varied either by the temperature of the water bath or of the gas pressure. Pressure and flow of the sample gas inside the ADM are controlled and maintained at optimum level using a gas flow meter (*GSC-B9TS-BB23, Vögtlin*), a needle valve and a vacuum pump (*N860.3 FT.40.18, KNF*). The flow of the gas mixture was kept at a constant flow of 250 ml min^{-1} for the dry sample gas and 100 ml min^{-1} for the humid sample gas mixtures, respectively.

3 Experimental results and discussion

3.1 Determination of optimum QEPAS operating parameters

The laser wavelength modulation depth m must be optimized at each pressure level in order to identify the optimum operating conditions in terms of the highest $2f$ WMS signal amplitudes, since the QEPAS sensor's sensitivity to the concentration of the trace gas component in a specific gas mixture is a function of the sample pressure. This two-parameter sensor optimization (p and m) was performed for two different gas mixtures:

- a dry reference gas mixture and
- a reference gas mixture moisturized with 2.3 % H_2O corresponding to a relative humidity of ~81 % at 23 °C and atmospheric pressure.

At each pressure level, the QTF parameters f_0 and Q were measured and the QEPAS laser modulation depth was varied in the range between 1 and 25 mA, which corresponded to 0.009 and 0.225 cm^{-1}.

The results of the $2f$ WM QEPAS signal amplitudes for different modulation depths are shown in Fig. 4. The optimum working pressure and modulation depth for a dry sample gas of 50 ppm SO_2:N_2 was found to be 175 mbar and 0.072 cm^{-1} and for 50 ppm SO_2 in moisturized N_2 (AH = 2.3 %) 100 mbar and 0.054 cm^{-1}, respectively. The difference between optimum working conditions for the two situations is due to the V–T relaxation mechanisms which are different in the two mixtures because of the different pressures and water content. In the dry gas mixture, the vibrational relaxation is slow, since the heat dissipation cannot efficiently follow the fast frequency modulation of the incident laser radiation. In this case, the optimum working conditions can be found at higher pressure levels, since an increase in the relaxation rate is achieved by an increase in the gas pressure. On the other hand, the QTF Q-factor decreases with increasing pressure, which causes the detected QEPAS signal to decrease [19].

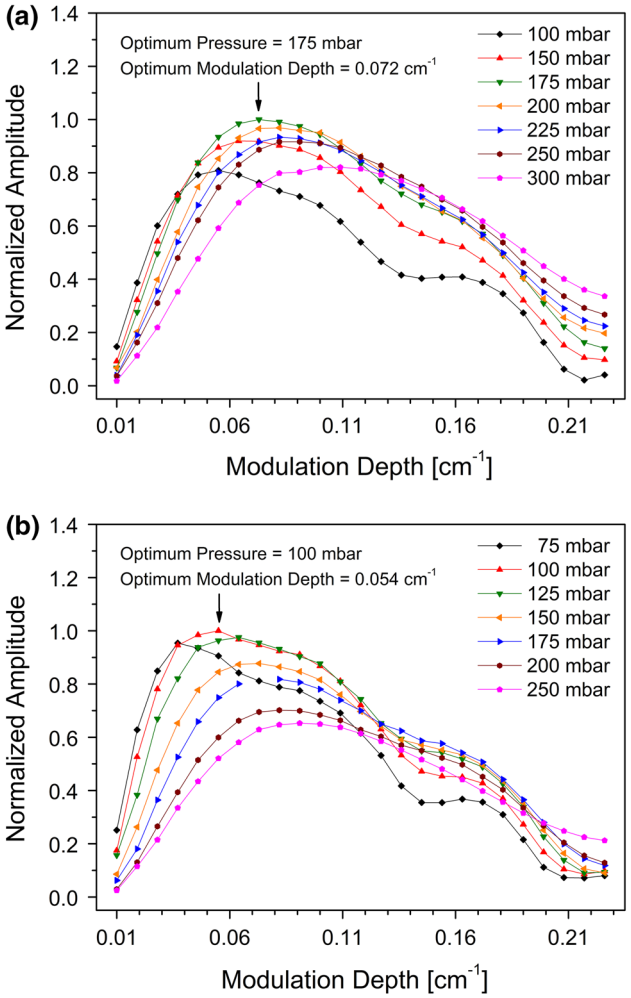

Fig. 4 Sensor optimization curves acquired at different operation pressures for **a** 50 ppm SO_2 in dry N_2 and **b** 50 ppm SO_2:N_2 moisturized with 2.3 % H_2O

Figure 4a shows the sensor optimization curves for a dry gas sample resulting from the competition of these two mechanisms. For a humid SO_2 gas mixture, the optimum working pressure shifted to lower pressure levels in respect to a dry gas mixture results. The presence of H_2O vapor influenced the QEPAS response to SO_2 by enhancing the V–T energy transfer rate. As previously, the QTF Q-factor increases at reduced pressures and the impact of these effects result in the sensor optimization curves shown in Fig. 4b. At optimum working pressure, the QTFs Q-factor shifted from ~27,958 to 33,448 and its resonance frequency shifted from f_0 = 32,756.78 to f_0 = 32,757.29 Hz, respectively.

3.2 Influence of water vapor on the SO_2 QEPAS signal

As discussed above, the presence of water vapor increases the relaxation rate of slow relaxing molecules such as SO_2

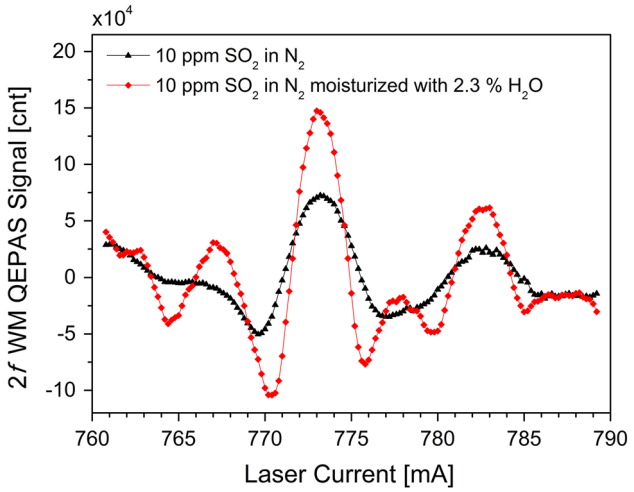

Fig. 5 2*f* WM QEPAS signals for 10 ppm SO_2 in dry N_2 (*black*) and moisturized N_2 with a 2.3 % H_2O mixture (*red*) when laser was tuned across absorption line located at 1,380.94 cm^{-1} at the optimum working condition for each: $p = 175$ mbar, $m = 0.072$ cm^{-1} (dry gas) and $p = 100$ mbar, $m = 0.054$ cm^{-1} (humidified gas), respectively

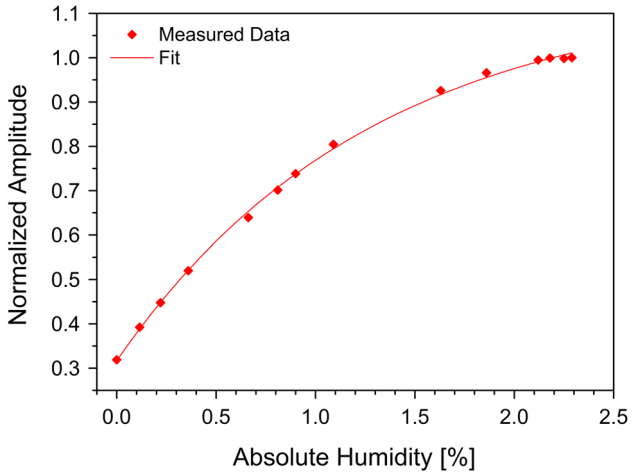

Fig. 6 2*f* WM QEPAS signal amplitudes of 50 ppm SO_2 as a function of H_2O concentration ($p = 100$ mbar, $m = 0.054$ cm^{-1})

and therefore improves the QEPAS response to SO_2 by increasing the signal amplitude. Figure 5 shows QEPAS spectra of 10 ppm SO_2 in dry N_2 and moisturized with 2.3 % water vapor mixture when the CW DFB-QCL emission wavelength was tuned across the SO_2 absorption line centered at 1,380.94 cm^{-1}. The measurements were performed at optimum operating conditions for each sample gas mixture, i.e., $p = 175$ mbar, $m = 0.072$ cm^{-1} for dry gas and $p = 100$ mbar, $m = 0.054$ cm^{-1} for humidified gas, respectively. A comparison of the measured results shows that a ~2.04 times improvement of the QEPAS signal amplitude was achieved when the absolute humidity of analyzed gas mixture was 2.3 %.

The dependence of the H_2O concentration on the response of the QEPAS-based SO_2 sensor system was investigated by acquiring 2*f* WMS signals of the 50 ppm SO_2 sample gas as a function of the H_2O concentration calibrated at the optimum working condition for a humid sample gas mixture ($p = 100$ mbar, $m = 0.054$ cm^{-1}). The results shown in Fig. 6 indicate an improvement of the QEPAS signal by a factor 3.13 when the absolute humidity of the analyzed gas mixture was 2.3 %.

3.3 Sensitivity and linear response of the QEPAS-based SO_2 sensor system

For the selected SO_2 absorption line centered at 1,380.93 cm^{-1}, the optical power emitted by the CW DFB-QCL was ~140 mW. The laser beam was focused between the mR and the gap of QTF prongs with a transmission efficiency of >97 %. The optical power measured at the focal point was ~52 mW due to optical power losses by the sensor system components, i.e., the aperture, the spatial filter and the CaF_2 lens. An optical power of ~48 mW was directed through the QTF prongs, when taking the absorption of the ZeSe window and the transmission efficiency into account.

The evaluation of the SO_2 QEPAS sensor sensitivity for dry and wet sample gas mixtures was investigated for both, a scan mode and a line-locked mode. The evaluation in the scan mode was performed by tuning the laser current from 760 to 790 mA which corresponded to a frequency tuning from 1,381.12 to 1,380.83 cm^{-1} and acquiring 2*f* WMS signal for dry and humidified gas mixture of 10 ppm SO_2:N_2 using a 1 s lock-in time constant and optimum operating settings for each mixture. The noise level was determined from the baseline recorded when the ADM was filled with dry and humidified nitrogen. The measurement results are illustrated in Fig. 5. The noise was calculated as the standard deviation of the measured data points, which yielded a value of $1\sigma = 2{,}907$ counts and $1\sigma = 3{,}506$ counts, respectively, for the scanned range. For a dry mixture of 10 ppm SO_2:N_2, the determined QEPAS SNR was 25, which resulted in a minimum detection limit (1σ) of 404 ppbv. For a humidified with 2.3 % water vapor mixture of 10 ppm SO_2:N_2, the measured SNR was 42, which yielded a minimum detection limit (1σ) of 238 ppbv. A normalized noise equivalent absorption coefficient NNEA $(1\sigma) = 9.90 \times 10^{-8}$ cm^{-1} W $Hz^{-1/2}$ and NNEA $(1\sigma) = 5.05 \times 10^{-8}$ cm^{-1} W $Hz^{-1/2}$ was obtained based on the corresponding detector bandwidth of 0.318 Hz and a QCL power of 48 mW between the prongs of the QTF (NNEA $= \alpha_{min} \cdot P \cdot \Delta f^{-1/2}$, where α_{min} is the minimum optical absorption coefficient, P the optical power and

Δf the detector bandwidth). However, the calculated noise values do not match the thermal noise level of the QTF at its resonance frequency, which is usually the dominating noise source limiting the device sensitivity. The noise determined from the baseline recorded for the ADM filled with N_2 at 100 and 175 mbar without any QCL radiation inside the mR yielded a value of $1\sigma \approx 350$ counts and $1\sigma \approx 430$ counts for the dry and wet sample gas. The measured noise was ~8.2–8.3 times higher compared to the typical thermal noise value of the QTF. For a dry and wet sample gas of 10 ppm SO_2:N_2, this noise level yielded a SNR of 207 and 343, respectively. The observed elevated noise levels may be due to the QCL illumination of the QTF. Radiation blocked by the QTF creates an undesirable background, which is several times larger than the noise level of the QTF and thus limits the QEPAS detection sensitivity. Hence, it is important to employ a high QCL beam quality in QEPAS. However, due to the QCL packaging, a laser interference pattern of the CW DFB-QCL beam profile was created, which resulted in a decreased beam quality. Despite a subsequent beam quality improvement by means of an external spatial filter, it was not possible to transmit the focused QCL beam through the gap of the QTF prongs without illuminating them. Therefore, additional QEPAS sensor noise was created by illumination of the inner surface of the mR and the QTF by the QCL radiation, including scattered light. The discrepancies between the SNR values determined for the QTF with and without illumination imply that the sensor performance can be improved by obtaining better QCL beam quality. The noise level of the illuminated QTF was also dependent on the value of the modulation amplitude in which the level was higher at higher modulation amplitudes. However, the measured noise level of the moisturized gas sample was ~20 % higher despite a lower modulation amplitude, which might results from different values for operating pressure, i.e., a reduced pressure of 100 mbar and therefore a higher associated Q-factor.

Quantitative measurements of SO_2 were performed using dry and moisturized SO_2 gas mixtures in order to investigate the sensitivity and linear response of the QEPAS sensor system in the line-locked mode. Different SO_2 concentration levels within a range from 0 to 10 ppm were achieved by diluting a 50 ppm SO_2:N_2 calibration mixture. Each concentration was measured three times in 60 s using a 1 s lock-in time constant. The data were averaged and plotted as a function of concentration which is shown in Fig. 7. Good linearity between signals amplitude and SO_2 concentrations is observed for the QEPAS-based sensor evaluating dry and moisturized gas mixtures at optimum operating conditions in each case (dry gas: $R^2 = 0.9998$, humidified gas: $R^2 = 0.9984$). The calculated noise of the measured data points recorded by the

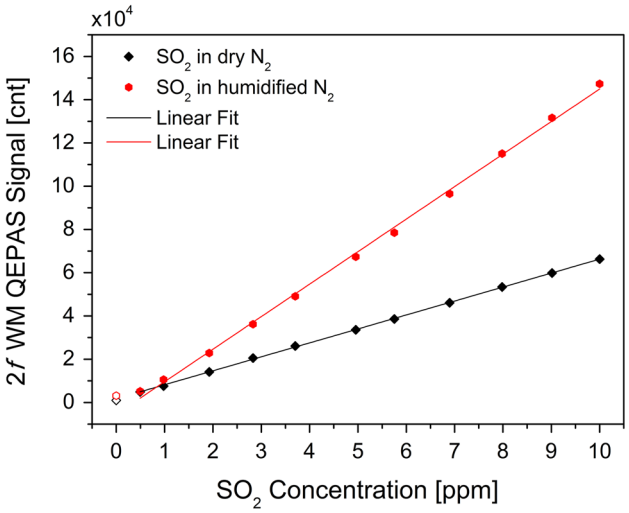

Fig. 7 Measured 2f WM QEPAS signal amplitudes as a function of SO_2 concentration (*black*: dry gas mixture, *red*: with 2.3 % absolute humidity moisturized gas mixture)

ADM filled with N_2 was $1\sigma = 676$ counts for the dry gas mixture and $1\sigma = 923$ counts for the moisturized sample, respectively. For a dry mixture of 10 ppm SO_2:N_2, the QEPAS SNR was 98, which yields a minimum detection limit (1σ) of 102 ppbv. For the same 10 ppm SO_2:N_2 mixture humidified with 2.3 % water vapor, the determined SNR was 160, which results in a minimum detection limit (1σ) of 63 ppbv. Moreover, for available 48 mW laser optical power between the QTF prongs, a NNEA (1σ) coefficient for a dry and moisturized gas mixture was calculated to be NNEA $(1\sigma) = 2.24 \times 10^{-8}$ cm^{-1} W Hz$^{-1/2}$ and NNEA $(1\sigma) = 1.21 \times 10^{-8}$ cm^{-1} W Hz$^{-1/2}$, respectively. Furthermore, the enhancement of relaxation process in the presence of H_2O vapor caused a substantial improvement of the QEPAS sensor system detection limit by a factor of ~1.62. In practical applications, the analyte often needs to be quantified in a gas mixture with unknown water content. In this case, the humidity can either be measured independently with a hygrometer, or the sample can be humidified before analysis. If the humidity is monitored with a sensor, the sensor detection sensitivity changes with the variation of the water content. Calibration data based on the present study can be used to convert measured values into actual analyte concentrations. In contrast, if the sample is humidified to nearby 100 % relative humidity before analysis, the sensor system sensitivity will be highest at optimum working conditions due to the enhancement of the V–T relaxation rate.

The corresponding limit of detection (LOD) was calculated with VALIDATA at three times the standard deviation of the intercept divided by the slope of the calibration curve, which resulted in 370 ppbv for dry sample gas and 300 ppbv for wet sample gas, respectively.

4 Conclusions

The results reported in this paper show that a CW DFB-QCL-based QEPAS sensor system offered sensitive detection of SO_2 sufficient for a number of practical applications, ranging from process control to environmental sensing. For the ν_3 SO_2 line centered at 1,380.93 cm^{-1}, a minimum detection limit of 63 ppbv ($\tau = 1$ s) was achieved when the gas sample was moisturized with 2.3 % water. This result corresponds to a normalized noise equivalent absorption coefficient of NNEA $(1\sigma) = 1.21 \times 10^{-8}$ cm^{-1} W $Hz^{-1/2}$. However, the detection sensitivity of this sensor configuration is limited by a nonoptimum DFB-QCL beam quality, resulting from packaging issues. It is most likely that in case of better QCL beam quality, the noise level can be further reduced down to a typical noise equivalent value of the QTF. Considering this option, the minimum detection limit could be lowered by a factor of $\sim$8.2 times. The achieved detection sensitivity along with the small required sample volume allows achieving fast sensor response to changes in the SO_2 concentration of injected gas streams.

Acknowledgments JPW, HM and MB acknowledge financial support provided by the Austrian research funding association under the scope of the COMET program within the research network "Process Analytical Chemistry" (contract # 825340) and the Carinthian Tech Research RL, FKT acknowledge financial support provided by NSF ERC MIRTHE and NSF-ANR NexCILAS.

References

1. R.F. Curl, F. Capasso, C. Gmachl, A.A. Kosterev, B. McManus, R. Lewicki, M. Pusharsky, G. Wysocki, F.K. Tittel, Chem. Phys. Lett. **487**, 1–18 (2010)
2. R. Lewicki, M. Jahjah, Y. Ma, P. Stefinski, J. Tarka, M. Razeghi, F. K. Tittel, Chap. 23 in *The Wonder of Nanotechnology: Quantum Optoelectronic devices and applications.* SPIE Press, pp. 597–632 (2013)
3. L. Gong, R. Lewicki, R. Griffin, F.K. Tittel, C.R. Lonsdale, R.G. Stevens, J.R. Pierce, Q.G.J. Malloy, S.A. Travis, L.M. Bobmanuel, B.L. Lefer, J.H. Flynn, Atmos. Environ. **77**, 893–900 (2013)
4. A. Varga, Z. Bozóki, M. Szakáll, G. Szabó, Appl. Phys. B **85**, 315–321 (2006)
5. S. Solga, T. Schwartz, M. Mudalel, L. Spacek, R. Lewicki, F. K. Tittel, C. Loccioni, T. Risby, J. Breath Res. **7**(3), 037101 (2013)
6. A. Miklós, P. Hess, Z. Bozóki, Rev. Sci. Instrum. **72**, 1937 (2001)
7. A.A. Kosterev, Y.A. Bakhirkin, R.F. Curl, F.K. Tittel, Opt. Lett. **27**, 1902–1904 (2002)
8. F. K. Tittel, R. Lewicki, Ch. 15, (Woodhead Publishing Ltd., 2013), pp. 579–629
9. V. Spagnolo, P. Patimisco, S. Borri, G. Scamarcio, B.E. Bernacki, J. Kriesel, Appl. Phys. B **112**, 25–33 (2013)
10. C. Bauer, U. Willer, R. Lewicki, A. Pohlkötter, A. Kosterev, D. Kosynkin, F.K. Tittel, W. Schade, J. Phys: Conf. Ser. **157**(1), 012002 (2009)
11. A.A. Kosterev, F.K. Tittel, D. Serebryakov, A.L. Malinovsky, I. Morozov, Rev. Sci. Instrum. **76**, 1–9 (2005)
12. A.A. Kosterev, Y.A. Bakhirkin, F.K. Tittel, Appl. Phys. B **80**, 133–138 (2005)
13. T.L. Cottrell, J.C. McCoubrey, *Molecular Energy Transfer in Gases* (Butterworths, London, 1961)
14. Pollution Prevention and Abatement Handbook (The World Bank Group, Washington DC, 1998)
15. L.S. Rothman, I.E. Gordon, Y. Babikov, A. Barbe, D. Chris Benner, P.F. Bernath, M. Birk, L. Bizzocchi, V. Boudon, L.R. Brown, A. Campargue, K. Chance, E.A. Cohen, L.H. Coudert, V.M. Devi, B.J. Drouin, A. Fayt, J.-M. Flaud, R.R. Gamache, J.J. Harrison, J.-M. Hartmann, C. Hill, J.T. Hodges, D. Jacquemart, A. Jolly, J. Lamouroux, R.J. Le Roy, G. Li, D.A. Long, O.M. Lyulin, C.J. Mackie, S.T. Massie, S. Mikhailenko, H.S.P. Müller, O.V. Naumenko, A.V. Nikitin, J. Orphal, V. Perevalov, A. Perrin, E.R. Polovtseva, C. Richard, M.A.H. Smith, E. Starikova, K. Sung, S. Tashkun, J. Tennyson, G.C. Toon, Vl.G Tyuterev, G. Wagner, J. Quant. Spectrosc. Radiat. Transf. **130**, 4–50 (2013)
16. L. Dong, A.A. Kosterev, D. Thomazy, F.K. Tittel, Appl. Phys. B **100**, 627–635 (2010)
17. S. Schilt, L. Thevenaz, Infrared Phys. **48**, 154–162 (2006)
18. R.D. Grober, J. Acimovic, J. Schuck, D. Hessman, P.J. Kindlemann, J. Hespanha, A.S. Morse, K. Karrai, I. Tiemann, S. Manus, Rev. Sci. Instrum. **71**, 2776–2780 (2000)
19. G. Wysocki, A.A. Kosterev, F.K. Tittel, Appl. Phys. B **85**, 301–306 (2006)